ROYAL SOCIETY
OF CHEMISTRY

PAPER

Comparison of bottom-up and top-down precipitation strategies for lignin nanoparticle obtention from organosolv and ionosolv *Eucalyptus globulus* liquors

Victoria Rigual, [ID] *[a] Antonio Ovejero-Pérez, [ID] [b] Antonio Martínez-Mangas,[a] Beatriz García-Sánchez, [ID] [a] Juan C. Domínguez, [ID] [a] M. Virginia Alonso, [ID] [a] Mercedes Oliet [ID] [a] and Francisco Rodriguez [ID] [a]

This work offers a side-by-side overview of the behaviour of two liquors obtained *via* two fractionation processes, ionosolv and organosolv, from *Eucalyptus globulus* wood, and how the precipitation strategy that follows may affect the final yield, morphology, and particle size of every kind of lignin nanoparticle. For lignin nanoparticle precipitation, two bottom-up techniques and two top-down approaches were employed to determine which combination of fractionation process and synthesis treatment would provide the nanoparticles with the best characteristics. The results demonstrated the importance of the fractionation process in the final lignin nanoparticle yield, as ionosolv fractionation gave enhanced yields of more than 60% lignin in the form of nanoparticles. However, sphericity, particle sizes, and non-agglomerated structures were easily obtained from organosolv liquors, in which precipitation was carried out progressively in the absence of sonication. The use of ultrasound mostly resulted in the breakage of particles into smaller and irregular pieces. However, in the case of ionosolv liquors, homogeneous spherical nanoparticles were fused, forming agglomerates of smaller particles through the top-down strategy of complete addition of the antisolvent followed by sonication. The highest precipitation yield of nanoparticles was obtained from ionosolv liquors in which the full amount of antisolvent was added in one step to precipitate lignin, and then sonication was applied. In contrast, the lignin nanoparticles (LNPs) precipitation strategy that resulted in more spherical LNPs was the bottom-up strategy of precipitation by progressive antisolvent addition, resulting in visually observed non-aggregated spherical particles with a particle size distribution of 200 nm < d_p < 500 nm, molecular weight of M_w = 14 000 g mol^{-1}, and thermal degradation property of $T_{10\%}$ = 310 °C.

[a]Department of Chemical Engineering and Materials, Complutense University of Madrid, 28040 Madrid, Spain. E-mail: vicrigua@ucm.es

[b]Department of Chemical Engineering, Imperial College London, South Kensington Campus, Exhibition Road, London SW7 2AZ, UK

1   Introduction

Non-edible lignocellulosic biomass is one of the most employed biomasses for biorefining since it is abundant and available and does not compete with the food sector. It presents a complex 3D structure, making pretreatment/fractionation needed for its exploitation *via* valorisation of its main components: cellulose, hemicellulose, and lignin.[1,2]

Lignin is the second most abundant natural biopolymer on the planet after cellulose. It is the main renewable source of aromatics, being present in all types of plants[3,4] It is an amorphous and three-dimensional polymer, with a complex structure that varies depending on the lignocellulosic material or biomass source used as feedstock, the process conditions, and the used extraction processes.[5,6] It is formed by the coupling of mainly three aromatic units from the corresponding phenylpropanoid-derived monomers, the three differing in the methoxylation degree of the main aromatic ring: the *p*-hydroxyphenyl unit (H, from *p*-coumaryl alcohol, non-methoxylated), guaiacyl unit (G, from coniferyl alcohol, C3-methoxylated), and syringyl unit (S, from sinapyl alcohol, C3 and C5-methoxylated).[7] These units are present in different proportions depending on the biomass source and the extraction method. G units are predominant in softwoods, whereas hardwood lignins present S and G units, and herbaceous lignins are formed by S, G, and H units.[8,9] These units are linked by C–O and C–C linkages having the aryl ether beta-O-4 as the predominant binding motif.[7,10]

Different processes have been employed for recovery delignification and pulp production, such as the Kraft, sulphite, or soda processes, among others.[11,12] Concretely, sulphite pulping is effective for delignification, although the lignins obtained are of low quality and sulphonated.[11,13] Two processes that can overcome some of these problems are the organosolv and ionosolv processes. The organosolv process employs organic solvents to solubilise lignin that can be recovered from the liquor *via* evaporation of the organic phase, also allowing the recovery of the employed solvents, and thus reducing the environmental impact.[14,15] On the other hand, the ionosolv process employs protic ionic liquids (ILs), organic salts whose melting points are below 100 °C and are easily synthesised *via* an acid–base neutralisation, to solubilise lignin, following mechanisms analogous to the organosolv process.[16,17] The lignin can be further precipitated *via* water addition, and the solvent can be recovered and reused through water distillation.[16] Apart from solvent recyclability, other advantages of the ionosolv processes are the possibility of tuning the IL by changing cation and/or anion to match the desired properties and the negligible vapor pressure during the process due to the nature of the solvent.[18,19]

It is estimated that between 50 and 70 million tons of lignin are produced every year.[20] Despite its high yearly production, the lignin fraction has been underutilised as it has typically been used for energy purposes; however, its valorisation into higher value-added products is considered one of the keys to obtaining a competitive biorefinery, although nowadays that valorization beyond energy purposes only represents 5% of the total lignin use.[4,21] Lignin uses alternative to burning have been proposed in the past few years, such as in binders, antioxidants, carbon fibre precursors, adhesives, and lubricant additives, but few of these applications have reached an industrial scale.[22–25]

The high heterogeneity and contamination of lignin (sugars or sulphur species in sulphur-based processes) hinder valorization. However, generating nano-materials from lignin is an interesting way to increase lignin valorisation opportunities.[26,27] Some of the proposed applications include UV protection products, coatings and paints, antimicrobials, drug carriers, and nano-composites, among others.[20,26–28]

Different methods for LNP synthesis have been proposed in the literature (ultrasonication, dialysis, antisolvent precipitation, polymerisation, *etc.*).[20,26] In most cases, the amphiphilic nature of lignin plays a major role in the LNP formation, with lignin particles forming micelles, where the hydrophilic part (hydroxyl and carboxyl groups) faces outwards and the hydrophobic part (phenylpropanoid units) faces inwards.[9] This structure can be obtained *via* either a bottom-up technique from the individual molecules arranging themselves into the nanostructure while they are precipitated, as happens in antisolvent precip-itation methods,[29] or by a top-down technique that consists of the breaking of a macroscopic material into the desired nanostructures, as in ultrasonication-based methods.[30]

In this work, we employed ionosolv and organosolv liquors from the frac-tionation of hemicellulose-free eucalyptus. For the formulation of LNPs, two bottom-up and two top-down techniques were compared, and the influence of ionosolv *vs.* organosolv liquors on the LNPs' yields and properties was investigated.

2 Materials and methods

2.1 Materials

Eucalyptus globulus wood was supplied by the Forestry Research Centre of the National Institute of Agricultural and Food Research and Technology (CIFOR-INIA). Prior to any treatment, eucalyptus wood was ground to a particle size of 0.2–2 mm. Before the organosolv or ionosolv fractionations, the eucalyptus wood was autohydrolysed following the optimised operational procedure ($S_0 = 3.81$) of our previous work.[31] The resulting pulp presented a composition of $34.33 \pm 1.26\%$ lignin, $64.98 \pm 1.85\%$ glucan, and $2.21 \pm 0.21\%$ xylan. This pulp was subsequently used for the organosolv and ionosolv treatments.

The reagents needed for IL synthesis, material characterisation, and the different analytical techniques followed in this work were purchased from Sigma-Aldrich with a purity always higher than 99%.

2.2 Ionic liquid synthesis

The IL ethanolammonium acetate was employed for ionosolv fractionation of the autohydrolysed pulp. It was synthesised *via* stoichiometric neutralisation of acetic acid and ethanolamine. In brief, the desired amount of ethanolamine was kept in a round-bottom flask placed in an ice bath. Acetic acid was added dropwise while stirring the mixture to ensure correct homogenisation and heat control. Once the addition was completed, the stirring was maintained for 2 h more. The target acid/base ratio was 1. Purity was measured *via* ^{1}H-NMR (Fig. S1) and the inte-gration of characteristic peaks (Table S1).

2.3 Obtaining black liquors from fractionation processes

Authohydrolysed eucalyptus was submitted to organosolv and ionosolv fractionation processes to obtain a lignin-rich liquor for use in LNPs synthesis. Preliminary studies with a liquid-to-solid ratio of 8 : 1 (g/g) for both ionosolv and organosolv processes were carried out, obtaining different precipitated lignin yields (52.03% and 43.77% for ionosolv and organosolv, respectively). However, to perform a proper comparison between treatments, the aim was for the lignin amount in the liquor to be the same in the ionosolv and organosolv fractionation processes. Considering the different lignin extraction yields of ionosolv and organosolv, the liquid-to-solid ratio was adjusted to obtain a similar absolute amount of lignin dissolved in the liquor obtained from both treatments.

2.3.1   Organosolv fractionation. Autohydrolysed eucalyptus was mixed with 60 wt% ethanol in a 7.3 : 1 solvent/solid ratio and placed in a stainless steel 450 mL Parr reactor, model 4567 (Parr Instrument Company, Moline, IL, USA) equipped with a Parr 4848 controller. The mixture was heated up to 200 °C over 50 min and then maintained at that temperature for 1 h. Then, it was cooled down at a cooling rate of 15 °C min^{-1}. Stirring was kept at 200 rpm. The slurry was filtered, and the cellulose pulp was separated from the black liquor.

2.3.2   Ionosolv fractionation. Autohydrolysed eucalyptus wood was mixed with dry ethanolammonium acetate in an 8.7 : 1 solvent/solid ratio and placed in a 250 mL Alamo glass reactor with overhead stirring. The mixture was heated up to 135 °C and kept under stirring at 60 rpm for 3 h. Once completed, the reactor was cooled down to 50 °C and a 50 wt% solution of acetone was added to recover and wash the cellulose pulp, which was separated from the black liquor via centrifugation.

The amount of the 50 wt% solution of acetone was sufficient to ensure that a clear liquid was obtained after cellulose pulp centrifugation.

Fig. 1 shows the experimental procedure to obtain the black liquors and the corresponding lignin mass balance. The ionosolv and organosolv black liquors contain different lignin concentrations but a similar absolute amount of lignin (3.7 g and 3.4 g for ionosolv and organosolv liquors, respectively). Working with the same or similar absolute amount of lignin is necessary to compare the precipitation yields of the fractionations. Yields of lignin extraction from biomass (e.g., eucalyptus) were 62% and 49% in the ionosolv and organosolv black liquors.

2.3.3   Base case lignin. Aliquots of both black liquors were used for complete lignin precipitation to have a base case of lignin. In the organosolv treatment, 3 g
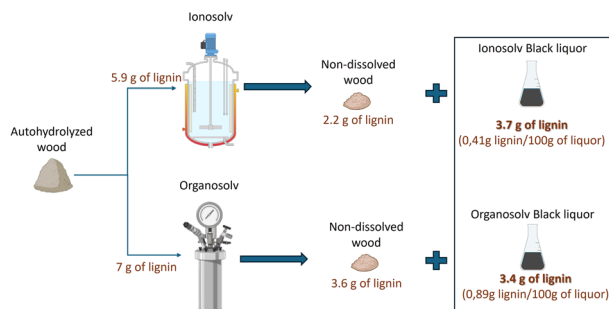

Fig. 1   Process scheme for the obtention of organosolv and ionosolv black liquors.

of water per g liquor (containing ethanol + water) was added, resulting in a lignin suspension containing 0.0023 g lignin per g solvent (containing ethanol + water). For the ionosolv lignin precipitation, the amount of water to add was adjusted to get a final suspension with the same lignin concentration as in the organosolv suspension (0.0023 g lignin per g solvent). Then, the lignins were washed with water and freeze-dried for further analysis. Samples were labelled as IO_BC and ORG_BC for ionosolv and organosolv base cases of lignin obtained with both treatments, respectively.

2.4 Lignin nanoparticle synthesis

Four different methods of LNP synthesis were tested in this study with both black liquors. The amount of water added for LNP precipitation (either in one step or multiple additions) was 3 g water per g black liquor for the organosolv treatment; however, for the ionosolv process, the amount of water to add was adjusted to keep the same lignin concentration in both treatments. In every case, after precipitation, the solids were recovered *via* centrifugation, washed, and freeze-dried for further analysis. A detailed nomenclature of every sample is shown in Table S2.

2.4.1 Ultrasonication + precipitation (bottom-up). In this configuration, the black liquors were sonicated while cooling using a Fisherbrand 505 probe for 1 h at 100 W and with a frequency of 20 Hz. After sonication, the total amount of water for precipitation was added to the liquors in a single step, and a solid was precipitated. Particles were labelled as IO_US and ORG_US for ionosolv and organosolv treatments, respectively.

2.4.2 Progressive addition of antisolvent (bottom-up). In this case, the amount of water that needed to be added for lignin precipitation was split into equal volumes that were added to the black liquor every 5 min over 1 h, while stirring. Particles were labelled as IO_PAA and ORG_PAA for ionosolv and organosolv treatments, respectively.

2.4.3 Progressive addition of antisolvent + ultrasonication (top-down). This configuration combines the previous two, as the amount of water was again split into equal volumes that were added every 5 min over 1 h, but sonication with the conditions listed before was applied at the same time. The recovered particles were labelled as IO_PAA+US and ORG_PAA+US for ionosolv and organosolv treatments, respectively.

2.4.4 Full precipitation + sonication (top-down). This case is the opposite of the bottom-up strategy. The full amount of water was added to the black liquors to precipitate lignin, and then sonication was applied to the suspensions for 1 h under the conditions listed before to form the LNPs. In this case, particles were labelled as IO_FP+US and ORG_FP+US for ionosolv and organosolv treatments, respectively.

2.5 Analytical methods

The recovered LNPs as well as the original lignins without treatment were characterised in terms of LNP yields, morphology, molecular weight distributions and average molecular weights, particle size distribution, and thermal stability.

2.5.1 Morphology. The morphology of the different LNPs was assessed in a JEOL JSM 7600F scanning electron microscope (SEM) at the Spanish National

Centre for Electron Microscopy (CNME). The microscope operated at 5 kV with a working distance of 8 mm. Prior to analysis, the particles were suspended in butanol at a 20 μg mL^{-1} concentration, and a brief ultrasound treatment was applied to generate a homogeneous dispersion of the LNPs within the solvent. Then, a drop of the suspension was placed in a metal holder, and butanol was evaporated prior to gold coating in a Q150 T turbo-pumped sputter coater to induce conductivity.

2.5.2 **Molecular weight distribution.** Gel permeation chromatography, to measure molecular weight distributions and average molecular weights, was conducted in an Agilent 1260 Infinity HPLC coupled with a Varian 390-LC viscometer detector. As two detectors (refractive index detector for concentration and viscometer for viscosity) were used, a universal polymer calibration was achieved, so the results presented were absolute.[32,33] Two Agilent PolarGel-M columns with a PolarGel precolumn were used. DMF + 1 g L^{-1} LiBr was used as the mobile phase at a 1 mL min^{-1} flow rate. The column compartment temperature, as well as detector temperatures, were set to 40 °C. ReadyCal Kit PMMA standards (M_w = 800–2 200 000 Da) from Polymer Standards Service GmbH were used for calibration. Every sample was prepared at a 2 mg mL^{-1} concentration and filtered through PTFE filters before analysis.

2.5.3 **Particle size distribution.** The particle size distribution and average particle size were measured using an ALV CGS-8 multiangle dynamic light scattering spectrometer at the Spectroscopy and Correlation unit of the Chemistry Faculty of the Complutense University of Madrid. LNPs were suspended at a 20 μg mL^{-1} concentration in butanol and briefly sonicated due to the tendency of LNPs to agglomerate.

2.5.4 **Thermal stability.** Thermal stability was measured via thermogravimetric analysis in a Mettler Toledo TGA/DSC 1 Star System. Approximately 7–10 mg samples were placed in sapphire crucibles, which were then heated up from 30 to 105 °C at 10 °C min^{-1} and maintained at 105 °C for 30 min for sample drying. Then, the temperature was increased from 105 to 950 °C at 10 °C min^{-1}. Nitrogen was used as the reaction and protection gas at 20 mL min^{-1} throughout the experiment.

3 Results and discussion

3.1 Mass balances and lignin precipitation yields of ionosolv and organosolv processes

Table 1 shows the most relevant yields of every fraction obtained in the ionosolv and organosolv fractionation processes.

Table 1 Lignin mass balance in the cellulose-rich solid and lignin of organosolv and ionosolv processes

	Ionosolv	Organosolv
Cellulose^a (pulp yield %)	78.0	79.7
Lignin yield^a (%)	18.8	15.9
Lignin recovered^b (%)	54.7	46.2

^{a} Percentage expressed per 100 g of AH wood. ^{b} Percentage expressed per 100 g of lignin in AH wood.

Through the proposed liquid-to-solid ratio, cellulose pulp yields of 78% and 80% were obtained for ionosolv and organosolv processes, respectively. The glucan contents of both cellulose pulps were 82 ± 1% and 76 ± 2% for the ionosolv and organosolv fractionation processes, respectively. The lignin contents in the cellulose pulps were 16 ± 1% and 22 ± 2% for the ionosolv and organosolv fractionation processes, respectively. This resulted in 64 g of cellulose extracted in cellulose pulp per 100 g of autohydrolyzed (AH) wood and 60 g of cellulose in cellulose pulp per 100 g of AH wood for the ionosolv and organosolv fractionation processes, respectively. As AH wood contains 65% cellulose, only 2% and 7% of the initial cellulose amount was not recovered as pulp in the ionosolv and organosolv treatments, respectively. In the same way, 62% and 49% of the initial lignin was present in the ionosolv and organosolv black liquors, being susceptible to precipitation. Although the conditions were not the same, even working at higher temperatures in the organosolv treatment, lower solubilities of lignin were obtained, which is in accordance with previous works that compared organosolv and ionosolv processes.[34] In a previous work, Ovejero-Pérez et al.[35] recovered 54% employing the ionic liquid 1-methylimidazolium chloride, which falls within the range of the results exposed in this work.[35] In the case of the organosolv fractionation process, results were in the range of those obtained with AH eucalyptus wood by Romaní et al.[14] Using an $S_0 = 3.64$, they precipitated 18%.

The precipitation yields of the base-case lignin as well as LNPs for every process are shown in Fig. 2. The compositional analysis using NREL/TP-510-42618 showed that in all the cases, no additional compounds were detected apart from lignin.[36] Previous literature reported a wide variety of LNPs yields in the range of 10–50%.[37–39] However, Fig. 2 shows that although organosolv LNPs may follow the same tendency, with LNP yields in the range of 9–24%, the precipitation yields of LNPs from ionosolv processes were even higher than those obtained for IO_BC (55%), with yields in the range of 56–63%. To the best of our knowledge, there is no previous literature about the obtention of LNPs from ionosolv black liquors. Thus, the use of ionosolv processes may empower the increase of LNP precipitation yields, independently of the strategy employed to precipitate those LNPs. From all the precipitation strategies tested, the highest
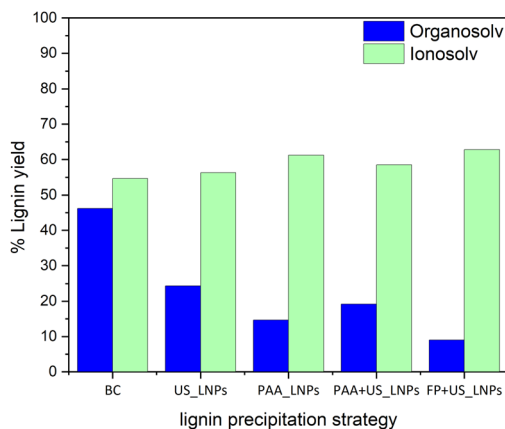

Fig. 2 LNP precipitated yield (%) expressed per 100 g of lignin in AH wood.

LNP yield was obtained through the IO_FP+US strategy, achieving a precipitation yield of 63% of the initial lignin present in AH wood in the form of LNPs.

3.2 LNP morphology

In Fig. 3, LNP micrographs of all the precipitated lignins are shown.

While in Fig. 3b the ORG_BC morphology already shows the presence of some particles with sphericity and particle sizes in the range of nanometres, in Fig. 3a IO_BC lignin clearly cannot be classified as LNPs as the scale bar is indicating
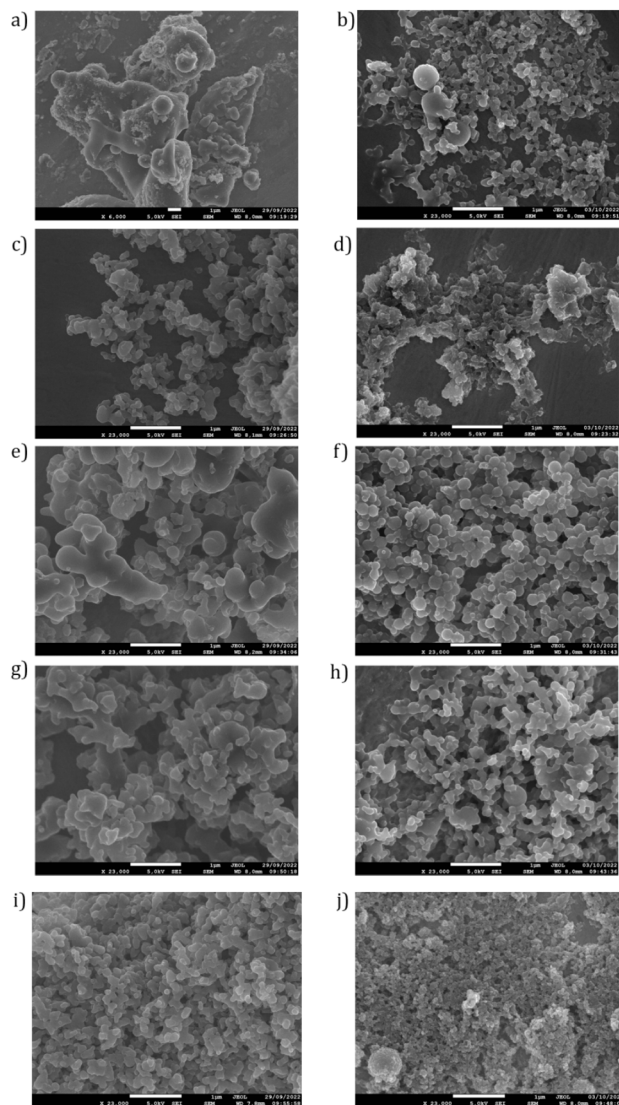

Fig. 3 SEM micrographs of (a) IO_BC; (b) ORG_BC, (c) IO_US; (d) ORG_US; (e) IO_PAA; (f) ORG_PAA; (g) IO_PAA+US; (h) ORG_PAA+US; (i) IO_FP+US; and (j) ORG_FP+US. The scale bar for all micrographs is 1 μm.

particles larger than 1 μm. Furthermore, the IO_BC lignins were irregular, according to the classification of Schneider et al.[20]

The bottom-up strategy of applying ultrasound and subsequently precipitating lignin *via* the addition of antisolvent clearly reduced the particle sizes of the solids, but non-spherical particles were obtained. LNPs were visualized as agglomerated, *i.e.*, fusing structures formed from non-well-defined individual particles. Comparing the "US" strategy with the base case, it was observed that although in the ionosolv liquor a reduction in the particle size was clearly shown (Fig. 3a *vs.* 3c), that reduction was not found for organosolv samples (Fig. 3b *vs.* 3d). In Fig. 3b, the LNPs are irregular, according to the classification of Schneider et al.[20]. According to Camargos and Rezende,[40] ultrasound leads to facilitated collisions of the LNPs, which causes non-uniform, non-spherical particles.[40] Those collisions resulted in non-uniform particles formed *via* the mechanism of mechanical exfoliations that were gradually removing layers of material.[20]

Micrographs of particles obtained *via* the bottom-up approach of progressive antisolvent addition are depicted in Fig. 3e (IO_PAA) and Fig. 3f (ORG_PAA). In Fig. 3e, independent nanospheres were not observed. Additionally, the particle size, despite being below one micrometre, was larger than those obtained through the application of ultrasound. Conversely, the ORG_PAA displayed homogeneous LNP distributions with consistently spherical structures. Of all the samples, the ORG_PAA micrographs exhibited the highest sphericity and homogeneity.

Micrographs of particles obtained through the top-down approach with subsequent ultrasound application are illustrated in Fig. 3g (IO_PAA+US) and Fig. 3h (ORG_PAA+US). The IO_PAA+US LNPs resembled those found in the top-down approach depicted in Fig. 3e, suggesting that the formation of LNPs through gradual antisolvent addition might have constrained subsequent fragmentation into smaller particles by sonication. The ORG_PAA+US samples appeared slightly smaller compared to those without ultrasound application (Fig. 3h *vs.* Fig. 3f). Furthermore, in this example, the ultrasound application seemed to have disrupted the stability of the LNPs obtained in Fig. 3f, leading to undesirable fused structures.

Lastly, the micrographs of particles obtained using the top-down approach involving the rapid addition of an antisolvent followed by ultrasound application are presented in Fig. 3i (IO_FP+US) and 3j (ORG_FP+US). The LNPs formed through the IO_FP+US method resulted in particles that were almost completely spherical and smaller, and exhibited higher sphericity compared to those observed using the IO_BC, IO_US, IO_PAA, and IO_PAA+US methods. It is hypothesized that once stable LNPs are formed, it is very challenging to fragment them into smaller particles. However, if the formation of LNPs is still ongoing, as is the case through the rapid addition of an antisolvent, the application of ultrasound may contribute to a reduction in particle size.

In contrast, Fig. 3j illustrates that the ORG_FP+US was granular, heterogeneous, and composed of small quasi-spherical particles likely formed through the fragmentation of larger particles. This observation aligns with the conclusions drawn by Camargos and Rezende.[40] The agglomeration led to the formation of fractal clusters, as observed during the synthesis from Klason lignin.[28]

3.3 LNPs molecular weights

Table 2 shows the weight-average and number-average molecular weights and the polydispersity of LNPs recovered, *via* the four different methods employed, from both black liquors and base-case lignins, calculated from the molecular weight distributions shown in Fig. S2 in the SI.

From Table 2, ionosolv LNPs presented higher molecular weight values than those obtained *via* the organosolv process, regardless of the LNP synthesis method, indicating greater depolymerisation followed by recondensation due to higher acidity of the ionosolv media. This led to higher agglomeration, as shown by the SEM micrographs, due to a higher phenolic hydroxyl content and thus a higher hydrophilicity.[40] This behaviour was already seen when Ovejero-Pérez *et al.*[34] compared ionosolv and organosolv treatments for poplar fractionation.[34] The higher values of M_w and M_n obtained for ionosolv LNPs in comparison to organosolv LNPs are due to alcohols tending to react with the activated (cationic) lignin species and reducing recondensation. The PDI values were also almost always higher for the LNPs recovered from the ionosolv liquor compared to the LNPs recovered from the organosolv. It is also noticeable that the PDI values for the ionosolv LNPs differed much more than those for the organosolv LNPs, suggesting more heterogeneity in the ionosolv LNPs than in the organosolv LNPs. All the PDIs range between 7.3 and 13.9, which is a considerably higher PDI, but already observed by different authors.[35,41–46] The complexity of the process that lignin undergoes, together with the complex architecture of the lignin molecule (with different binding motifs, branches, *etc.*), may explain those high PDI values. The M_w values of the LNPs were slightly higher than those for the IO_BC sample. Considering the LNP formation (especially if only precipitation is involved) is merely a physical process, only the larger fragments of the lignin form the particles efficiently, whereas small molecules tend to stay in solution, without being considered in the M_w determination.

The M_w values of the organosolv LNPs (11 090–14 000 g mol^{-1}) were higher than the M_w of the ORG_BC (8790 g mol^{-1}). The proposed LNP synthesis methods slightly increased the molecular weights but not the heterogeneity of the sample. Comparing the M_w of the different LNP synthesis methods, all of them presented very similar values, being just slightly higher in the PAA. These two samples also presented the highest PDI values, suggesting that the progressive addition of

Table 2 Weight-average (M_w, g mol^{-1}) and number-average (M_n, g mol^{-1}) molecular weights and polydispersity index (PDI) of lignin samples

	M_n (g mol^{-1})	M_w (g mol^{-1})	PDI
IO_BC	1740	24 200	13.9
IO_US	2370	26 930	11.4
IO_PAA	3070	29 100	9.5
IO_PAA+US	2620	30 490	11.6
IO_FP+US	3120	27 680	8.9
ORG_BC	1020	8790	8.6
ORG_US	1430	12 370	8.7
ORG_PAA	1550	14 000	9.0
ORG_PAA+US	1470	13 680	9.3
ORG_FP+US	1510	11 090	7.3

water gave the dissolved lignin more time to precipitate, as opposed to the samples in which water was added in a single addition.[34]

LNPs recovered from the ionosolv liquor showed a similar behaviour, with higher molecular weights in the PAA samples (M_w of around 30 000 Da and high PDI). This could be due to the longer times for the lignin to precipitate, in contrast to the one-time addition of water. The use of sonication could have also promoted further fragmentation, giving rise to more heterogeneous LNPs (see also IO_US). Comparing the SEM micrographs, higher molecular weights showed higher agglomeration (Fig. 2e and g), due to an increase of hydrophilicity.[41]

Molecular weight distributions of the LNPs are shown in Fig. S2 of the SI. The ionosolv samples showed very similar distributions with a single maximum, except for IO_BC, which showed a broader distribution and the coexistence of two closely positioned maxima. The differences observed indicate that the lignin modification was independent of the LNP formation mechanism. For the orga-nosolv LNPs, the distributions only showed slight differences among them, indicating that the LNP synthesis method did not generate large differences between the obtained LNPs, which agrees with the discussion above.

3.4 LNP particle size

The particle size distributions for the recovered LNPs from both liquors with the four different LNP synthesis methods are shown in Fig. 4. Notice that the particle size evolved with the time of analysis (as shown in Fig. S3 in the SI for the case of IO_BC as an example), showing particle instability *via* agglomeration. Therefore, all the analyses shown here were taken at short times, after suspension in butanol and sonication for 30 seconds, before agglomeration started.

All the statistical distributions of the ionosolv LNPs, except the IO_PAA+US sample ($400 \leq d_p \leq 1100$ nm), were below 1 μm, which verifies that the samples obtained were made up of nanometre-sized particles ($d_p \leq 500$ nm). The IO_PAA+US sample was one of the most condensed ones (see previous section). However, the IO_PAA sample, which presented a high molecular weight distri-bution, showed a narrow peak and a lower particle size distribution than the rest of the samples. These results contradict what was shown in the molecular weight distribution. We hypothesize that in this particular case, the agglomeration was so intense that, even with short-time sonication, the particles were not sus-pended. As a result, they sank to the bottom of the Eppendorf tube, and only the smaller suspended fragments were analysed. In consequence, the results from the IO_PAA sample should be taken carefully.

The curves obtained for the methods that employed one-time addition of water (IO_US, IO_FP+IS) were very similar to each other ($150 \leq d_p \leq 400$ nm), and very close to that of IO_BC lignin, indicating unsuccessful LNP synthesis.

For the organosolv LNPs, the curves obtained for the ORG_PAA and ORG_F-P+US samples were very similar to each other ($200 \leq d_p \leq 500$ nm) and the largest among the organosolv samples, which agreed with what was seen in the micro-graphs (Fig. 3f and j). All the samples presented homogeneous particle size distributions, with relatively narrow peaks ($200 < d_p < 300$ nm), owing to a more stable structure of the LNPs with time due to the lower agglomeration of lignin (and lower acidity of the liquor, as explained before). The smallest particle sizes were obtained with two sonication-based methods (ORG_US and ORG_PAA+US),
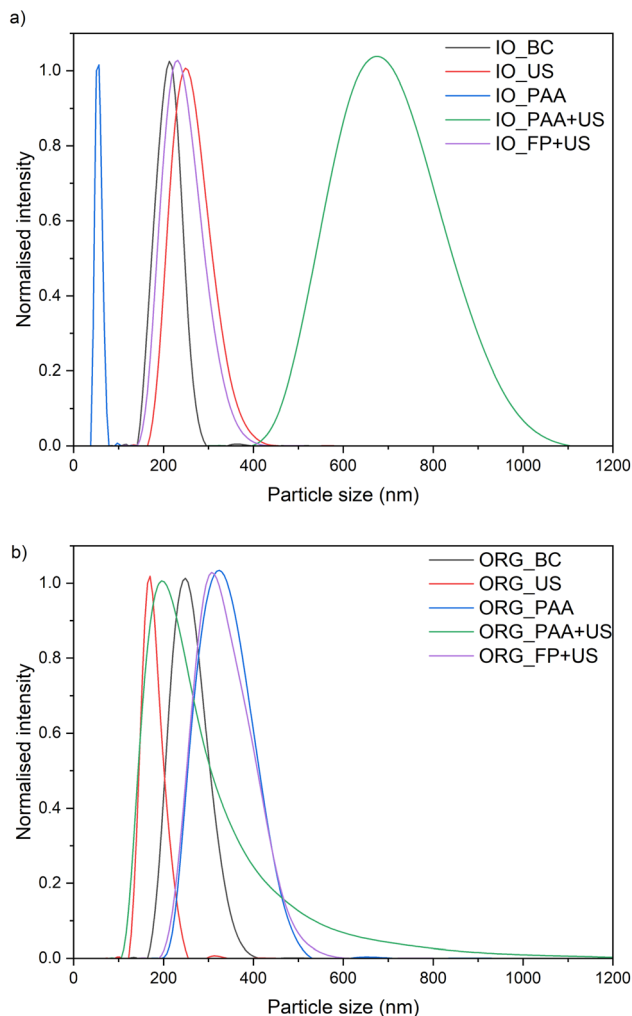
Faraday Discussions | Paper

a)

b)

Fig. 4 Particle size distributions of LNPs and base-case lignins from (a) ionosolv treatment, and (b) organosolv treatment.

achieving smaller LNPs than in the base case. The lower M_w achieved for organosolv LNPs (in comparison with ionosolv LNPs) and the application of ultrasound enhanced the breakage of lignin into smaller fragments. In fact, those visually smaller particles can be appreciated in the SEM images (Fig. 3d and h). In the case of the ORG_PAA+US, a tailing is observed, probably as a consequence of agglomeration during the DLS measurements.

3.5 Thermal stability of lignin nanoparticles

Fig. S4 and S5 in the SI show thermograms of all the precipitated lignin samples, while in Table 3 the main parameters of each thermogram are shown.

The thermograms of ionosolv lignins and organosolv lignins exhibited considerable intra-group similarity, with the exceptions of IO_BC and ORG_BC, which deviated from the general thermal behaviour of their categories. In the case

This journal is © The Royal Society of Chemistry 2026

Table 3 Main temperature parameters of the thermal degradation and ash contents (at 800 °C) of precipitated lignins. $T_{10\%}$ and $T_{50\%}$ are defined as the temperatures at which the sample loses 10% and 50% of the initial mass, respectively; $T_{P1, P2, and P3}$ are defined as the temperatures at which a change in the slope of the TG curve is observed

Sample name	$T_{10\%}$ (°C)	$T_{50\%}$ (°C)	T_{P1} (°C)	T_{P2} (°C)	T_{P3} (°C)	Ash content$_{800°C}$ (%)
IO_BC	318	436	367	—	—	33.7
IO_US	310	593	359	—	—	43.4
IO_PAA	306	604	354	—	—	43.3
IO_PAA+US	304	587	351	—	—	43.4
IO_FP+US	299	579	352	—	—	43.2
ORG_BC	329	628	358	371	—	43.5
ORG_US	301	522	337	355	368	37.7
ORG_PAA	310	545	341	362	—	38.7
ORG_PAA+US	308	551	332	346	361	39.4
ORG_FP+US	306	531	352	368	—	38.2

of organosolv lignins, the obtained thermal stabilities were in the range of other precipitated organosolv lignins, varying according to the extraction conditions.[47]

IO_BC and ORG_BC samples were more stable with T_{P1} and $T_{10\%}$ values of 367 and 358 °C, and 318 and 329 °C, respectively. Although the T_{P1} of ORG_BC was lower than for IO_BC, after 400 °C there was a sharp loss of weight of the IO_BC sample, reaching the lowest ash content of all the samples (33.7%). In comparison, the ash contents of all the ionosolv LNPs, besides the IO_BC sample, were higher (43.2–43.4%). The thermal stability (T_{P1} and $T_{10\%}$) of LNPs obtained from the organosolv process was lower than for ORG_BC, with an ash content within the range of 37.7–39.4%. The degradation of ionosolv LNPs took place in a single step, whereas LNPs obtained with organosolv showed several peaks in their thermograms. Additionally, the slopes (mass loss rate) observed in the thermograms of ionosolv LNPs were slightly milder than for organosolv LNPs. Furthermore, the $T_{50\%}$ values were in the range of 579–604 °C for ionosolv LNPs, while in the case of LNPs from the organosolv process, the $T_{50\%}$ values were in the range of 522–551 °C. Previous work of Ovejero-Pérez et al.[35] employing the IL 1-methylimidazolium chloride resulted in a lignin with a $T_{10\%}$ of 293 °C, which is slightly lower than the $T_{10\%}$ obtained in this work for IO_BC (318 °C) and the precipitated LNPs ($T_{10\%}$ in the range of 299–310 °C).[35]

4 Conclusions

This work shows a side-by-side comparison of lignin nanoparticle obtention from ionosolv and organosolv black liquors following bottom-up and top-down strategies. Organosolv LNPs had molecular weights lower (11 095 g mol^{-1} < M_w < 14 002 g mol^{-1}; 7.33 < PDI < 9.29) and more homogeneous than those of ionosolv LNPs (26 957 g mol^{-1} < M_w < 30 493 g mol^{-1}; 8.86 < PDI < 11.38). Furthermore, the sphericity of the organosolv LNPs was higher and the surfaces were softer than in LNPs. However, the LNP precipitation yield of ionosolv LNPs (56.6–63.1%) was considerably higher than in organosolv LNPs (9.0–19.2%). The LNP precipitation strategy that resulted in more spheric LNPs was the progressive precipitation of antisolvent to organosolv liquors, resulting in particles with a particle size

distribution of 200 nm $< d_p <$ 500 nm; molecular weight of $M_w = 14\ 000$ g mol^{-1}; $M_n = 1550$ g mol^{-1}; PDI = 9.04; and thermal stability properties of: $T_{10\%} = 310$ °C; $T_{50\%} = 545$ °C; % ashes at 800 °C = 38.7%. This work may be helpful as an initial basis for the selection of the best biomass fractionation technique (ionosolv or organosolv) and the best LNP precipitation strategy to obtain certain amounts of LNPs with certain characteristics, such as morphology or particle size distribution, according to the final application of the LNPs.

Author contributions

Victoria Rigual: conceptualization, data curation, formal analysis, and writing the original draft. Antonio Ovejero-Pérez: conceptualization, data curation, methodology, supervision, and writing the original draft. Antonio Martínez-Mangas: formal analysis and investigation. Beatriz García-Sánchez: formal analysis and investigation. Juan C. Domínguez: supervision and funding acquisition. Mercedes Oliet: funding acquisition and project administration. M. Virginia Alonso: supervision and validation. Francisco Rodriguez: funding acquisition.

Conflicts of interest

There are no conflicts to declare.

Data availability

The data supporting this article have been included as part of the SI. See DOI: https://doi.org/10.1039/d5fd00070j.

Acknowledgements

References

1 D. Haldar and M. K. Purkait, *Chemosphere*, 2021, **264**, 128523.

2 B. Prasad, R. Padhi and G. Ghosh, *Int. J. Environ. Sci. Technol.*, 2023, **20**, 6929–6944.

3 J. Becker and C. Wittmann, *Biotechnol. Adv.*, 2019, **37**, 107360.

4 M. Lievonen, J. J. Valle-Delgado, M.-L. Mattinen, E.-L. Hult, K. Lintinen, M. A. Kostiainen, A. Paananen, G. R. Szilvay, H. Setälä and M. Österberg, *Green Chem.*, 2016, **18**, 1416–1422.

5 S. Laurichesse and L. Avérous, *Prog. Polym. Sci.*, 2014, **39**, 1266–1290.

6 W. Zhao, L.-P. Xiao, G. Song, R.-C. Sun, L. He, S. Singh, B. A. Simmons and G. Cheng, *Green Chem.*, 2017, **19**, 3272–3281.

7 J. Ralph, K. Lundquist, G. Brunow, F. Lu, H. Kim, P. F. Schatz, J. M. Marita, R. D. Hatfield, S. A. Ralph, J. H. Christensen, *et al.*, *Phytochem. Rev.*, 2004, **3**, 29–60.

8   C. Li, X. Zhao, A. Wang, G. W. Huber and T. Zhang, *Chem. Rev.*, 2015, **115**, 11559–11624.

9   D. Tian, J. Hu, R. P. Chandra, J. N. Saddler and C. Lu, *ACS Sustainable Chem. Eng.*, 2017, **5**, 2702–2710.

10 W. Boerjan, J. Ralph and M. Baucher, *Annu. Rev. Plant Biol.*, 2003, **54**, 519–546.

11 E. Melro, A. Filipe, D. Sousa, B. Medronho and A. Romano, *New J. Chem.*, 2021, **45**, 6986–7013.

12 P. Azadi, O. R. Inderwildi, R. Farnood and D. A. King, *Renewable Sustainable Energy Rev.*, 2013, **21**, 506–523.

13 D. Ekeberg, K. S. Gretland, J. Gustafsson, S. M. Bråten and G. E. Fredheim, *Anal. Chim. Acta*, 2006, **565**, 121–128.

14 A. Romaní, G. Garrote, F. López and J. C. Parajó, *Bioresour. Technol.*, 2011, **102**, 5896–5904.

15 Z. Zhou, F. Lei, P. Li and J. Jiang, *Biotechnol. Bioeng.*, 2018, **115**, 2683–2702.

16 P. Y. Nakasu, P. V. Barbará, A. E. Firth and J. P. Hallett, *Trends Chem.*, 2022, **4**, 175–178.

17 A. Brandt, J. Gräsvik, J. P. Hallett and T. Welton, *Green Chem.*, 2013, **15**, 550–583.

18 D. J. van Osch, L. J. Kollau, A. van den Bruinhorst, S. Asikainen, M. A. Rocha and M. C. Kroon, *Phys. Chem. Chem. Phys.*, 2017, **19**, 2636–2665.

19 Y. Cao, R. Zhang, T. Cheng, J. Guo, M. Xian and H. Liu, *Appl. Microbiol. Biotechnol.*, 2017, **101**, 521–532.

20 W. D. H. Schneider, A. J. P. Dillon and M. Camassola, *Biotechnol. Adv.*, 2021, **47**, 107685.

21 D. Koch, M. Paul, S. Beisl, A. Friedl and B. Mihalyi, *J. Clean. Prod.*, 2020, **245**, 118760.

22 M. Culebras, H. Geaney, A. Beaucamp, P. Upadhyaya, E. Dalton, K. M. Ryan and M. N. Collins, *ChemSusChem*, 2019, **12**, 4516–4521.

23 H. Wang, Y. Pu, A. Ragauskas and B. Yang, *Bioresour. Technol.*, 2019, **271**, 449–461.

24 A. M. Borrero-López, R. Martín-Sampedro, D. Ibarra, C. Valencia, M. E. Eugenio and J. M. Franco, *Int. J. Biol. Macromol.*, 2020, **162**, 1398–1413.

25 T.-Q. Yuan, F. Xu and R.-C. Sun, *J. Chem. Technol. Biotechnol.*, 2013, **88**, 346–352.

26 S. Iravani and R. S. Varma, *Green Chem.*, 2020, **22**, 612–636.

27 B. Wang and D. Sun, *Chem. Eng.*, 2019, **7**, 2658–2666.

28 W. Zhao, B. Simmons, S. Singh, A. Ragauskas and G. Cheng, *Green Chem.*, 2016, **18**, 5693–5700.

29 C. Frangville, M. Rutkevičius, A. P. Richter, O. D. Velev, S. D. Stoyanov and V. N. Paunov, *ChemPhysChem*, 2012, **13**, 4235–4243.

30 I. A. Gilca, V. I. Popa and C. Crestini, *Ultrason. Sonochem.*, 2015, **23**, 369–375.

31 A. Ovejero-Pérez, V. Rigual, J. C. Domínguez, M. V. Alonso, M. Oliet and F. Rodriguez, *RSC Adv.*, 2023, **13**, 10338–10348.

32 Z. Grubisic, P. Rempp and H. Benoit, *J. Polym. Sci. B: Polym. Lett.*, 1967, **5**, 753–759.

33 J. D. Timpa, *J. Agric. Food Chem.*, 1991, **39**, 270–275.

34 A. Ovejero-Pérez, V. Rigual, J. C. Domínguez, M. V. Alonso, M. Oliet and F. Rodriguez, *Int. J. Biol. Macromol.*, 2022, **197**, 131–140.

35 A. Ovejero-Pérez, V. Rigual, J. C. Domínguez, M. V. Alonso, M. Oliet and F. Rodriguez, *RSC Adv.*, 2023, **13**, 10338–10348.

36 A. Sluiter, B. Hames, R. Ruiz, C. Scarlata, J. Sluiter, D. Templeton and D. Crocker, Determination of structural carbohydrates and lignin in biomass, *NREL Technical Report*, 2012.

37 R. M. F. de Mesquita, W. D. H. Schneider, V. Longo, H. M. Baudel, E. Diebold, J. Rencoret, A. Gutiérrez, A. Cavaco-Paulo, A. Ribeiro and M. Camassola, *Int. J. Biol. Macromol.*, 2025, **306**, 141676.

38 H. Trevisan and C. A. Rezende, *Ind. Crops Prod.*, 2020, **145**, 112105.

39 Z. Zhang, V. Terrasson and E. Guénin, *Nanomaterials*, 2021, **11**, 1336.

40 C. H. Camargos and C. A. Rezende, *Int. J. Biol. Macromol.*, 2021, **193**, 647–660.

41 J. D. Zwilling, X. Jiang, F. Zambrano, R. A. Venditti, H. Jameel, O. D. Velev, O. J. Rojas and R. Gonzalez, *Green Chem.*, 2021, **23**, 1001–1012.

42 J. Li, G. Henriksson and G. Gellerstedt, *Bioresour. Technol.*, 2007, **98**, 3061–3068.

43 L. Weigand, S. Mostame, A. Brandt-Talbot, T. Welton and J. P. Hallett, *Faraday Discuss.*, 2017, **202**, 331–349.

44 Y. Sun and B. Xue, *Ind. Crops Prod.*, 2018, **123**, 600–609.

45 A. Brandt, L. Chen, B. E. van Dongen, T. Welton and J. P. Hallett, *Green Chem.*, 2015, **17**, 5019–5034.

46 T. C. Pin, L. B. Brenelli, V. M. Nascimento, A. C. Costa, Y. Pu, A. J. Ragauskas and S. C. Rabelo, *Ind. Crops Prod.*, 2021, **159**, 113080.

47 J. Domínguez, M. Oliet, M. V. Alonso, M. Gilarranz and F. Rodríguez, *Ind. Crops Prod.*, 2008, **27**, 150–156.